Hindawi
Advances in Materials Science and Engineering
Volume 2017, Article ID 6310321, 13 pages
https://doi.org/10.1155/2017/6310321

Research Article

Impact of Plastic Hinge Properties on Capacity Curve of Reinforced Concrete Bridges

Nasim Shatarat,[1] Mutasem Shehadeh,[2] and Mohammad Naser[3]

[1]*Civil Engineering Department, The University of Jordan, Amman 11942, Jordan*
[2]*Department of Mechanical Engineering, American University of Beirut, Beirut, Lebanon*
[3]*The Hashemite University of Jordan, Zarqa, Jordan*

Correspondence should be addressed to Nasim Shatarat; n.shatarat@ju.edu.jo

Received 15 February 2017; Revised 16 May 2017; Accepted 6 June 2017; Published 16 August 2017

Academic Editor: Jun Liu

Pushover analysis is becoming recently the most practical tool for nonlinear analysis of regular and irregular highway bridges. The nonlinear behaviour of structural elements in this type of analysis can be modeled through automated-hinge or user-defined hinge models. The nonlinear properties of the user-defined hinge model for existing highway bridges can be determined in accordance with the recommendations of the Seismic Retrofit Manual by the Federal Highway Administration (FHWA-SRM). Finite element software such as the software SAP2000 offers a simpler and easier approach to determine the nonlinear hinge properties through the automated-hinge model which are determined automatically from the member material and cross section properties. However, the uncertainties in using the automated-hinge model in place of user-defined hinge model have never been addressed, especially for existing and widened bridges. In response to this need, pushover analysis was carried out for four old highway bridges, of which two were widened using the same superstructure but with more attention to seismic detailing requirements. The results of the analyses showed noticeable differences in the capacity curves obtained utilizing the user-defined and automated-hinge models. The study recommends that bridge design manuals clearly ask bridge designers to evaluate the deformation capacities of existing bridges and widened bridges using user-defined hinge model that is determined in accordance with the provisions of the FHWA-SRM.

1. Introduction

Several methods are available to capture the seismic behaviour of buildings and highway bridges. These methods range from simple equivalent static analysis to complex nonlinear dynamic analysis. Nonlinear time-history analysis constitutes the most reliable approach to estimate seismic behaviour because it can realistically predict the deformation demand on and capacity of structures, especially for irregular ones. However, complexities in the application of this method limit its use by practicing engineers [1]. The nonlinear static procedure often called "Pushover analysis" appears therefore as an interesting alternative approach due to its simplicity, yet ensuring reasonably accurate results [2].

Pushover analysis is not a recent development and its origin traces back to 1970s [3]. The validity and applicability of pushover analysis to seismic assessment of buildings and highway bridges have been extensively investigated in literature [4–13]. Currently, pushover analysis is a very common method of analysis among the structural engineering profession and researchers and is recommended by most guidelines and codes, such as in FEMA 273 [14], ATC-40 [15], FEMA 356 [16], Eurocode 8 [17], FEMA-440 (ATC-55) [18], and ASCE/SEI 41-06 Standard [19].

In pushover analysis, the results depend on the approach used to define the plastic hinges, whether it is lumped or distributed plasticity model [2]. Concentrated plasticity is the most commonly used approach for estimating the deformation capacity in the seismic codes, manuals, and structural analysis software [2, 20]. However, a proper definition of the concentrated plastic hinge model depends on many factors such as mechanical properties of longitudinal and transverse reinforcement, reinforcement details, reinforcement ratio, concrete compressive strength, cross-sectional shape, axial

force level, level of confinement, plastic hinge length, and possible local failure mechanisms within the plastic hinge zone [21–23]. Practically, most often the nonlinear properties recommended by FEMA-356 [16], ATC-40 [15], and Caltrans [24] documents are used to describe the deformation capacity of the plastic hinge without any consideration to possible local failure mechanisms due to convenience and simplicity [20].

Many commercial software programs are available to perform pushover analysis. A survey on engineering firms showed that the software SAP2000 [25] is the most used software by bridge engineers for nonlinear static analysis of highway bridges [2]. In SAP2000, the nonlinear behaviour of structural elements for pushover analysis can be modeled through automated-hinge or user-defined hinge models. The nonlinear properties of the user-defined hinge model for existing highway bridges can be determined in accordance with the recommendations of the FHWA-SRM [26], which provides the most current state-of-practice for evaluating the seismic vulnerability of old and existing highway bridges. The document demonstrates detailed procedures for calculating the curvature capacity of the structural elements based on potential local failure mechanisms within the plastic hinge. On the other hand, the nonlinear properties of the automated-hinge model may be based on FEMA-356, Caltrans specifications, or can be determined automatically from the member material and cross section properties.

The literature review showed that very limited research is available on the possible differences in the capacity curve when using user-defined versus automated-hinge models. Inel and Ozmen [20] investigated the influence of different plastic hinge properties on the capacity curve of four- and seven-storey reinforced concrete buildings. The results of their study showed that the improper use of default-hinge model could lead to displacement capacities that might be unreasonable. The authors concluded that the user-defined hinge model is better than the default-hinge model as it reflects nonlinear behaviour compatible with the element properties. It is worth noting that this study was explicitly oriented to reinforced concrete buildings and that default-hinge properties were defined based on FEMA-356. Furthermore, user-defined hinge properties were obtained from moment-curvature analysis based on extreme compression fiber reaching the ultimate concrete compressive strain, as determined by Priestley et al. [1], or the longitudinal steel reaching a tensile strain of 50% of the ultimate strain capacity.

Shatarat [27] studied the effect of plastic hinge properties on the capacity curve of highway bridges. A bridge that was built in the 1940s was considered for the purpose of the study. The curvature capacity of the plastic hinge zone was controlled by buckling of longitudinal rebars. Pushover analysis was carried out for the bridge in one direction only using user-defined and automated plastic hinge models. The results of the study showed a difference in the capacity curve when using the two different models. However, the study was limited to one bridge with one type of local failure mechanism of the plastic hinge zone.

Due to the growing use of pushover analysis in seismic assessment of old highway bridges, there is a need to assess the suitability of utilizing automated plastic hinge properties, which is based on material and section properties, as an alternative to user-defined plastic hinge properties that are determined based on FHWA-SRM for obtaining bridge capacity curves utilizing the software SAP2000. This paper addresses that need by examining the capacity curves of four highway bridges that were built in the 1960s, of which two were widened in 1980s, using two alternatives in defining the properties of the plastic hinge zone. The four bridges were selected to represent old bridges and widened bridges and to cover all types of possible local failure mechanisms within the plastic hinge zone.

2. Plastic Hinge Local Failure Mechanisms

According to the FHWA-SRM [26], the plastic curvature capacity of a reinforced concrete element should be based on the controlling limit state of the potential plastic hinge zone, shear strength of the member, and strength of the joint. Shear strength of the members and the joints is not addressed in this study. A complete discussion of these limit states is covered in the FHWA-SRM [26]. However, a summary of the equations corresponding to each limit state is given in Table 1.

3. Pushover Analysis

3.1. User-Defined Plastic Hinge Properties. For user-defined hinge properties, moment-curvature relationship and the axial-moment interaction surface of the potential plastic hinge are determined by the user and input into the software SAP2000. A minimum of five axial load levels are required to define the interaction surface. An elastic perfectly plastic moment-curvature relationship is established for each axial load level based on the controlling plastic curvature limit state that is determined in accordance with the FHWA-SRM [26]. For axial load levels other than the five values used to create the interaction surface, the software SAP2000 uses linear interpolation to determine the plastic hinge curvature. Plastic hinge length and location are determined in accordance with the FHWA-SRM [26] and are input by the user. MathCAD sheets [28] were developed to handle the large amount of calculations under this part.

3.2. Automated Plastic Hinge Properties. For this model, the moment-curvature relationship and the axial-moment interaction surface of the potential plastic hinge are determined by the software SAP2000. The parameters required for generating moment-curvature relationship and interaction surface compromise the definition of the column cross section geometry, longitudinal and transverse reinforcement details, and unconfined concrete and steel stress-strain curve parameters. Unconfined stress-strain parameters are set based on the expected concrete strength and strain levels as required in the AASHTO guide specifications for LRFD Seismic Bridge Design [29]. Longitudinal and transverse stress-strain parameters are set based on the expected strengths following the models suggested by Caltrans specifications. Mander et al. [30] confined concrete stress-strain curve of the column

Table 1: Curvature limit states.

Failure criteria	Plastic curvature (ϕ_p)
Compression failure of unconfined concrete	$\phi_p = \frac{\xi_{cu}}{c} - \phi_y$
Compression failure of confined concrete	$\phi_p = \frac{\varepsilon_{cu}}{(c - d'')} - \phi_y$
Buckling of longitudinal bars	$\phi_p = \frac{2f_y}{E_s(c - d')} - \phi_y \; 6d_b < s < 30d_b$
Fracture of the longitudinal reinforcement	$\phi_p = \frac{\varepsilon_{s\max}}{(d - c)} - \phi_y$
Low cycle fatigue of longitudinal reinforcement	$\phi_p = \frac{2\varepsilon_{ap}}{D'}$
Failure in the lap-splice zone	$\phi_p = (\mu_{lap\phi} + 7)\phi_y$

ξ_{cu} is the ultimate concrete compression strain for unconfined concrete and is limited to 0.005; c is the distance from the extreme compression fiber to the neutral axis; ϕ_y is the yield curvature given by the following equation: $\phi_y = 2\varepsilon_y/D'$; ε_y is equal to the expected yield strength of the longitudinal reinforcement f_{ye} divided by the modulus of elasticity; D' is the length between the center lines of the transverse reinforcement; d'' is distance measured from centerline of the perimeter stirrup to the extreme compression fiber of the cover concrete; ε_{cu} is the ultimate strain of the confined concrete and is determined by $\varepsilon_{cu} = 0.005 + 1.4\rho_s f_{yh}\varepsilon_{su}/f'_{cc}$; ε_{su} is strain corresponding to the maximum stress of the transverse rebars; f_{yh} is yield stress of the transverse steel; ρ_s is volumetric ratio of transverse steel; f'_{cc} is confined concrete strength; d' is the distance from the extreme compression fiber to the centroid of the nearest compression rebars; ε_{smax} is limited to a value of 0.10 or less and d is the effective depth of the cross section; ε_{ap} is plastic strain amplitude, as given by $\varepsilon_{ap} = 0.08(2N_f)^{-0.5}$; N_f is given by $N_f = 3.5(T_n)^{-1/3}$ provided that: $2 \le N_f \le 10$; T_n is natural period of vibration of the bridge; l_{lap} is the length of the lap-splice that is provided; l_s is the lap-splice length $l_s = 0.4(f_{ye}/\sqrt{f'_{ce}})d_b$; L_p is plastic hinge length. $L_p = [0.08L + 4400\varepsilon_y d_b]$ and $L_p = l_{lap}$ if l_{lap} is smaller than l_s; f'_{ce} is the expected strength of concrete surrounding the lap-splice zone; L is the shear length of the member; $\mu_{lap\phi}$ is the curvature ductility at the initial breakdown of bond in the lap-splice zone.

core is consequently generated based on the aforementioned parameters. The software divides the cross section into fiber elements to generate the moment-curvature relationship. The plastic hinge length and its relative location are taken identical to user-defined hinge properties.

4. Description of Selected Bridges

A preliminary evaluation of plastic hinge properties was performed on a group of old bridges that were built in early 1960s with little attention to seismic forces and reinforcement details. This step helped in selecting four candidates that would have different local failure mechanisms within the potential plastic hinge zones. Two of the selected bridges were widened with same superstructure; however the substructure received more attention to seismic detailing requirements. The following is a description of the selected bridges.

4.1. Bridge #1-W Description. Bridge #1-W was originally built in 1961 and consists of four simply supported spans supported on three intermediate piers. The original superstructure consisted of precast concrete girders with span lengths of 60 ft, 98 ft, 98 ft, and 80 ft (3.28 ft = 1 m). The original roadway width was 27 ft with a 6 ft wide sidewalk. The intermediate piers are supported on three 3-ft circular columns that are connected through a beam of 4.5 ft height. The intermediate piers are constructed on isolated footings, while the bridge abutments are seat type abutments supported on concrete piles. In 1983, the roadway was widened by 45 ft to an overall width of 72 ft and the sidewalk was expanded by 6 ft, to an overall width of 12 ft. At each intermediate pier, the new precast concrete girders are supported on four columns, each having a diameter of 3 ft. Unlike the original columns, longitudinal reinforcement lap splices were removed from the plastic hinge zone and the transverse reinforcement was changed to spiral reinforcement with a larger bar size. Table 2 shows columns' geometric properties, concrete strength, and reinforcement details.

4.2. Bridge #2-E Description. Bridge #2-E consists of three simply supported spans totaling 213 ft in length, with a 22-ft roadway width. The superstructure consists of precast concrete girders supported by 45-degrees skewed intermediate piers that are comprised of two circular 3-ft diameter columns constructed on footings with timber piles. The bridge abutments are seat type abutments founded on precast concrete piles. Poor seismic detailing of the column ends showed the existence of a lap splice of the longitudinal reinforcement within the potential plastic hinge zone with a length of 40 in. Also, the transverse reinforcement consisted of #3 hoop rebars that are spaced at 12.0 in. Table 3 shows columns' geometric properties, concrete strength, and reinforcement details.

4.3. Bridge #3-E Description. Bridge #3-E consists of a 4.5-ft deep multicell cast-in-situ reinforced concrete box girder with spans of 47, 73, 73, and 47 feet. The bridge roadway width is 49 ft with two 6-ft wide sidewalks. The intermediate Piers 2 and 4 are comprised of four square 2.5 ft columns, while intermediate Pier 3 is comprised of four rectangular 2.0 ft by 2.5 ft columns. The bridge abutments are spill-through type abutments with four square 2.5 ft columns hinged at the top and bottom in the bridge longitudinal direction. The columns of the abutments and the intermediate Piers are founded on square spread footings. Column longitudinal reinforcement was spliced in the potential plastic hinge zone with poor

Table 2: Bridge #1-W columns' geometric properties and reinforcement details*.

	Pier #2		Pier #3		Pier #4	
	Old	Widened	Old	Widened	Old	Widened
Column						
Clear length (ft)	28.6	25.8	32.2	29.2	26.8	24.2
Shape	Circular	Circular	Circular	Circular	Circular	Circular
Dimensions (in.)	36	36	36	36	36	36
Compressive strength (ksi)	4.0	4.0	4.0	4.0	4.0	4.0
Longitudinal reinforcement						
Size and number	12#9	12#9	12#9	12#9	12#9	12#9
Yield strength (ksi)	40	60	40	60	40	60
Transverse reinforcement						
Type	Hoop	Spiral	Hoop	Spiral	Hoop	Spiral
Size and number	#3	#4	#3	#4	#3	#4
Spacing (in.)	12.0	3.3	12.0	3.3	12.0	3.3
Lap splice						
Within plastic hinge	Yes	No	Yes	No	Yes	No
Length (in.)	50.0	—	50.0	—	50.0	—

*(1 in. = 25.4 mm; 1 ksi = 6.89 MPa).

Table 3: Bridge #2-E columns' geometric properties and reinforcement details.

	Pier #2	Pier #3
Column		
Clear length (ft)	20.75	19.50
Shape	Circular	Circular
Dimensions (in.)	36	36
Compressive strength (ksi)	4.0	4.0
Longitudinal reinforcement		
Size and number	12#9	12#9
Yield strength (ksi)	40	40
Transverse reinforcement		
Type	Hoop	Hoop
Size and number	#3	#3
Spacing (in.)	12.0	12.0
Lap splice		
Within plastic hinge	Yes	Yes
Length (in.)	40.0	40.0

transverse confinement that is comprised of a single #3 hoop spaced at 12 in on centre. Table 4 shows columns' geometric properties, concrete strength, and reinforcement details.

4.4. Bridge #4-W Description. Bridge #4-W consists of three simply supported spans, totaling 260 ft in length. The roadway width was 44 ft before widening. The superstructure is comprised of precast concrete girders, with span lengths of 78 ft, 93 ft, and 89 ft. Each intermediate pier is comprised of five 3-ft diameter circular columns supported by single footings. The bridge abutments are seat type abutments founded on spread footings. The roadway was widened by 23 ft to an overall width of 67 ft. This bridge widening included the addition of precast concrete girders and two 3-ft diameter columns founded on 4.5-ft diameter shafts at each intermediate bent. The original and new column longitudinal reinforcements were spliced within the potential plastic hinge zone. However, column transverse confinement was improved through the use of #4 spiral reinforcement spaced at 3.0 in. on centre. Table 5 shows columns' geometric properties, concrete strength, and reinforcement details.

5. Modeling of the Selected Bridges

A three-dimensional spine-type model was created for each bridge, as shown in Figure 1 for Bridge #2-E. The superstructure and pier elements are represented by frame elements that pass through their centroid. The columns are split into three frame elements as required by Section 5.4.3 of the AASHTO Guide Specifications for LRFD Seismic Bridge Design. Effective moments of inertia were used to reflect concrete cracking and reinforcement yielding, as provided in Table 7-1 of the FHWA-SRM [26]. Gross section properties were used for the elements representing the super structure, the cross beam, and the foundation as they are assumed to behave elastically. Figure 2 shows a typical bridge pier, the frame elements, and their associated stiffness. Spread footings were represented by spring elements which were determined utilizing the method for spread footings outlined in the FHWA-SRM [26]. L-pile software [31] was used to generate equivalent linear-elastic springs for the piles.

A modal analysis was performed to identify fundamental natural periods and mode shapes. Pushover analysis was then carried out for each pier individually and independently in

Table 4: Bridge #3-E columns' geometric properties and reinforcement details.

	Pier #2	Pier #3	Pier #4
Column			
Clear length (ft)	22.5	22.0	21.5
Shape	Square	Rectangular	Square
Dimensions (in.)	30	Width = 30 Depth = 24	30
Compressive strength (ksi)	4.0	4.0	4.0
Longitudinal reinforcement			
Size and number	8#10	8#9	8#10
Yield strength (ksi)	40	40	40
Transverse reinforcement			
Type	Hoop	Hoop	Hoop
Size and number	1#3	1#3	1#3
Spacing (in.)	12.0	12.0	12.0
Lap splice			
Within plastic hinge	Yes	Yes	Yes
Length (in.)	50.0	44.0	50.0

Table 5: Bridge #4-W columns' geometric properties and reinforcement details.

	Pier #2 and Pier #3	
	Old	Widened
Column		
Clear length (ft)	26.0	26.0
Shape	Circular	Circular
Dimensions (in.)	36	36
Compressive strength (ksi)	4.0	4.0
Longitudinal reinforcement		
Size and number	12#9	13#10
Yield strength (ksi)	40	60
Transverse reinforcement		
Type	Hoop	Spiral
Size and number	#3	#4
Spacing (in.)	12.0	3.0
Lap splice		
Within plastic hinge	Yes	Yes
Length (in.)	40	40

both the longitudinal and the transverse direction, as per the requirements of the FHWA-SRM [26].

6. Approach for Studying the Effect of Plastic Hinge Properties

Accurate determination of the nonlinear capacity curve of a highway bridge depends on the properties of the plastic hinge zone. Typically, design documents and seismic manuals proposed plastic hinge properties based on mechanical properties of longitudinal and transverse reinforcement, reinforcement details, reinforcement ratio, concrete compressive

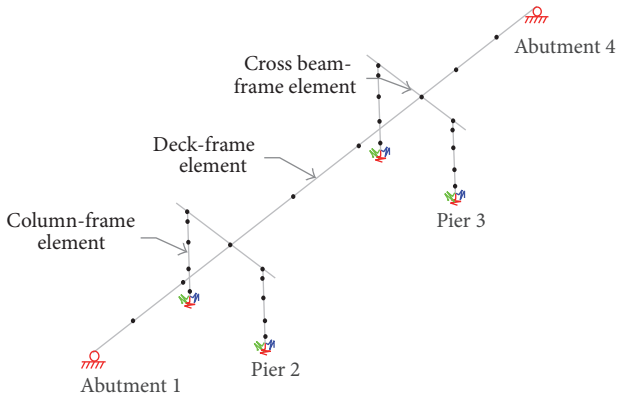

Figure 1: Three-dimensional model of Bridge #2-E.

strength, cross-sectional shape, axial force level, and level of confinement. The FHWA-SRM [26] is the only document to include the effect of possible local failure mechanisms in the hinge zone on the properties of the hinge model. The following summarizes the approach used in this study to determine the capacity curve based on user-defined and automated plastic hinge properties:

(1) A three-dimensional model was created to determine the natural periods of the selected bridges.

(2) For user-defined plastic hinge properties, the curvature capacity of each limit state for each pier column at three axial load levels: balanced point P_b, dead and seismic loads P_s, and pure flexure P_f, in the transverse and longitudinal directions, is determined using the in-house developed MathCAD sheets.

(3) The ordinates of the moment-curvature relationships at the associated axial load levels, axial-moment interaction surface, and plastic hinge length were

Table 6: Plastic curvature capacity of Pier #2 old columns, Bridge #1-W*.

Axial load level	Axial force** (kips)	Direction	Compression failure Unconfined	Buckling of long. rebars	Fracture of long. rebars	Low-cycle fatigue of long. rebars	Failure in the lap-splice zone
				rad/in.			
P_b	−1543.0	T & L	0.0002197	**0.0001173**	0.0056480	0.0020726	0.0011435
P_s	−584.0	T	0.0004549	**0.0003543**	0.0040599	0.0020726	0.0014724
P_s	−302.0	L	0.0006400	**0.0006224**	0.0037028	0.0020726	0.0017314
P_f	0.0	T & L	**0.0011457**	0.0024662	0.0033434	0.0020726	0.0024387

*1 kip = 4.45 kN; 1 k·ft = 0.00135 kN·m; ** P_o = −3868.6 kips and P_t = 782.6 kips.

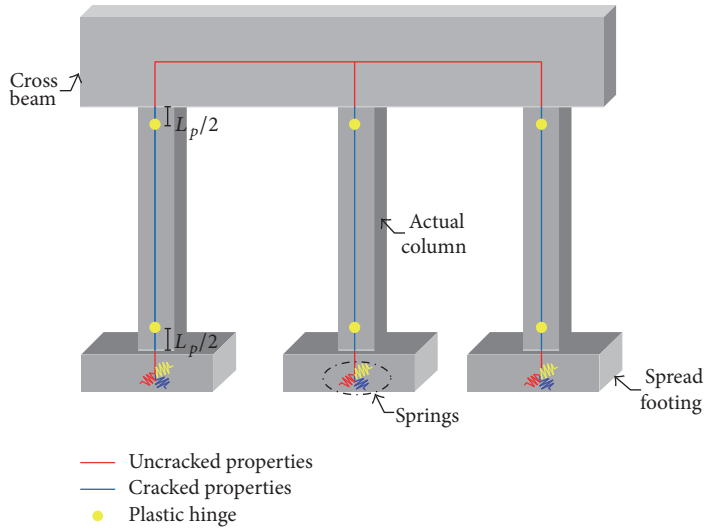

Figure 2: Bridge pier elements and associated stiffness.

input into the software SAP2000 under user-defined plastic hinge properties.

(4) The capacity curve using user-defined hinge properties was obtained by pushing each pier individually and independently in both the longitudinal and the transverse direction, as per the requirements of the FHWA-SRM.

(5) For automated plastic hinge properties, the moment-curvature relationship and the axial-moment interaction surface of the potential plastic hinge are determined by the software SAP2000 based on the column cross section geometry, longitudinal and transverse reinforcement details, and unconfined concrete and steel stress-strain curve parameters.

(6) The capacity curve using automated plastic hinge properties was obtained by pushing each pier individually and independently in both the longitudinal and the transverse direction.

(7) Capacity curves using user-defined and automated plastic hinge properties were then compared and discussed.

7. Analysis Results and Discussions

For user-defined plastic hinge properties, the value of the controlling limit state is shown in bold type font. Plastic curvature and plastic rotation for pure compression P_o and pure Tension P_t are not included because they are equal to zero. The ordinates of the moment-curvature relationships at the associated axial load levels, axial-moment interaction surface, and plastic hinge length to be input into the software SAP2000 are shown in Tables 6, 7, 8, and 9.

7.1. Bridge #1-W. Pier #2, Pier #3, and Pier #4 columns showed similar behaviour in regard to curvature capacity limit states. Therefore, for brevity, results for Pier #2 are reported. It is clear from Table 6 that buckling of longitudinal rebars is the controlling limit state of the columns of the old piers at P_b and P_s axial load levels in both directions. This behaviour is attributed to the poor confinement details, #3 hoops at 12.0 in. spacing. As the axial load decreases and reaches zero, P_f, compression failure of the unconfined concrete becomes the controlling limit state. The unconfined concrete in here refers to the cover concrete and the core concrete. The change in the type of the controlling limit state supports the effect of the axial load level on the deformation capacity of the plastic

Table 7: User-defined plastic hinge properties of Pier #2 old columns, Bridge #1-W.

Direction	Axial load level	Overstrength Axial (kips)	Overstrength Moment (kip·ft)	Plastic hinge length (L_p) (in.)	Yield curvature rad/in$*10^{-6}$	Yield rotation Rad	Plastic curvature rad/in$*10^{-6}$	Plastic rotation Rad
T	P_b	−1543.0	1554.4	21.18	99.6	0.00211	**0.0001173**	0.00248
	P_s	−584.0	1290.1				**0.0003543**	0.00750
	P_f	0.0	870.2				**0.0011457**	0.02427
L	P_b	−1543.0	1554.4	34.91	99.6	0.00348	**0.0001173**	0.00409
	P_s	−302.0	1111.8				**0.0006224**	0.02173
	P_f	0.0	870.2				**0.0011457**	0.04000

Table 8: Plastic curvature capacity of Pier #2 widened columns, Bridge #1-W.

Axial load level	Axial Force* (kips)	Direction	Compression failure confined	Buckling of long. rebars	Fracture of long. rebars	Low-cycle fatigue of long. rebars	Failure in the lap-splice zone
			rad/in.				
P_b	−1705.7	T & L	**0.0011781**	NA**	0.0055760	0.0020899	NA
P_s	−584.0	T	0.0025015	NA	0.0040056	**0.0020899**	NA
P_s	−302.0	L	0.0035630	NA	0.0037024	**0.0020899**	NA
P_f	0.0	T & L	0.0068851	NA	0.0033970	**0.0020899**	NA

*$P_o = -4585.3$ kips and $P_t = 1174.0$ kips; **NA = Not applicable.

Table 9: User-defined plastic hinge properties of Pier #2 widened columns, Bridge #1-W.

Direction	Axial load level	Overstrength Axial (kips)	Overstrength Moment (kip·ft)	Plastic hinge length (L_p) (in.)	Yield curvature rad/in$*10^{-6}$	Yield rotation Rad	Plastic curvature rad/in$*10^{-6}$	Plastic rotation rad
T	P_b	−1705.7	1958.51	23.57	150.6	0.00355	**0.0011781**	0.02776
	P_s	−584.0	1661.35				**0.0020899**	0.04925
	P_f	0.0	1271.37				**0.0020899**	0.04925
L	P_b	−1705.7	1958.51	35.95	150.6	0.00541	**0.0011781**	0.04235
	P_s	−302.0	1493.15				**0.0020899**	0.07513
	P_f	0.0	1271.37				**0.0020899**	0.07513

hinge. Also, the values of the controlling curvature capacities shown in Table 6 identify the effect of the axial force on the deformation capacity of the plastic hinge. For example, the curvature capacity was equal to 0.0001173 rad/in at axial force of 1543.0 kips and 0.0011457 rad/in. at zero axial force level. Table 7 shows the moment-curvature ordinates and the moment-axial force interaction surface.

The columns of the new piers had confined concrete details where transverse reinforcement consisted of #4 spirals at 3.3 in. and column longitudinal reinforcement was not spliced within the plastic hinge zone. Therefore, buckling of longitudinal rebars and failure in the lap splice zone are not applicable, as shown in Table 8. Accordingly, low cycle fatigue of longitudinal rebars was the controlling limit state at P_s and P_f axial load levels, while compression failure of the confined concrete controlled the curvature capacity at P_b axial load level. Failure limit state pertaining to unconfined concrete is not considered for the widened columns because the core concrete has the capability to withstand higher plastic curvature demands after spalling off the cover concrete. Comparison of curvature capacities between the old and the new columns shows the effect of the confinement on the deformation capacity of the plastic hinge. For example, the plastic curvature capacity of the old column was 0.0011457 rad/in, while the curvature capacity of the new column was 0.0020899 rad/in. at the zero axial load level.

Tables 7 and 9 show that the plastic hinge length in the transverse direction is less than the plastic hinge length in the longitudinal direction which is basically attributed to the difference in the shear span in both directions. Subsequently, higher deformation capacities are expected in the longitudinal direction. It should be noted that the plastic hinge length was determined in accordance with the equations in the FHWA-SRM which depends on the

Table 10: Plastic curvature capacity of Pier #2 columns, Bridge #2-E.

Axial load level	Axial Force* (kips)	Direction	Compression failure unconfined	Buckling of long. rebars	Fracture of long. rebars	Low-cycle fatigue of long. rebars	Failure in the lap-splice zone
			rad/in.				
P_b	−1543.0	T & L	0.0002197	**0.0001173**	0.0056480	0.0020010	0.0011435
P_s	−405.0	T	0.0005576	**0.0004913**	0.0038295	0.0020010	0.0016161
P_s	−302.0	L	0.0006404	**0.0006231**	0.0037024	0.0020010	0.0017319
P_f	0.0	T & L	**0.0011457**	0.0024662	0.0033434	0.0020010	0.0024387

* P_o = −3868.6 kips and P_t = 782.6 kips.

shear span of the member, and the yield strain and the diameter of the longitudinal bars. However, other researchers [21, 23] identified that the plastic hinge length depends on the axial load level, aspect ratio of the member, type of reinforcement, longitudinal and transverse reinforcement ratios, and concrete strength.

Figures 3 and 4 show the capacity curves of Bridge #1-W in the longitudinal and transverse directions, respectively. The figures also show the capacity curves based on user-defined and automated plastic hinge properties. It is clear from Figure 3 that the base shear capacity of Pier #2, Pier #3, and Pier #4 in the longitudinal direction using the automated-hinge model is less than base shear capacity using user-defined hinge model by 17.7%, 15.2%, and 15.4%, respectively. On the other hand, the displacement capacity of Pier #2, Pier #3, and Pier #4 in the longitudinal direction using the automated-hinge model is higher than the displacement capacity using user-defined hinge model by 9.7%, 18.9%, and 9.7%, respectively. Similarly, Figure 4 shows that base shear capacity of Pier #2, Pier #3, and Pier #4 in the transverse direction using the automated-hinge model is less than base shear capacity using user-defined hinge model by 15.9%, 15.7%, and 16.0%, respectively. However, the displacement capacity of Pier #2, Pier #3, and Pier #4 in the transverse direction using the automated-hinge model is higher than the displacement capacity using user-defined hinge model by 10.9%, 20.2%, and 15.0%, respectively.

The differences in the base shear and displacement capacities of the bridge piers using the two hinge models are retained to the differences in the associated moment-curvature relationship. At an axial load level of −584.0 kips, P_s, the ultimate curvature capacity is equal to 6.33 × 10^{-4} rad/in. and the associated idealized moment capacity is equal to 1155.4 k·ft using the automated-hinge model in SAP2000. The corresponding values using the user-defined model are equal to 3.54 × 10^{-4} rad/in. and 1290.1 k·ft, respectively.

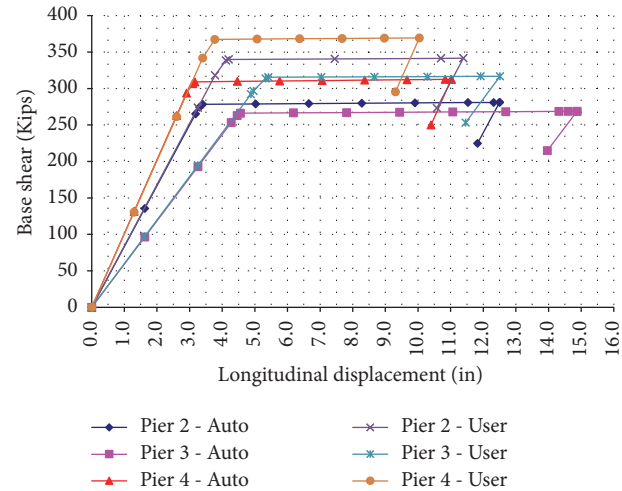

Figure 3: Longitudinal pushover capacity curve of Bridge #1-W.

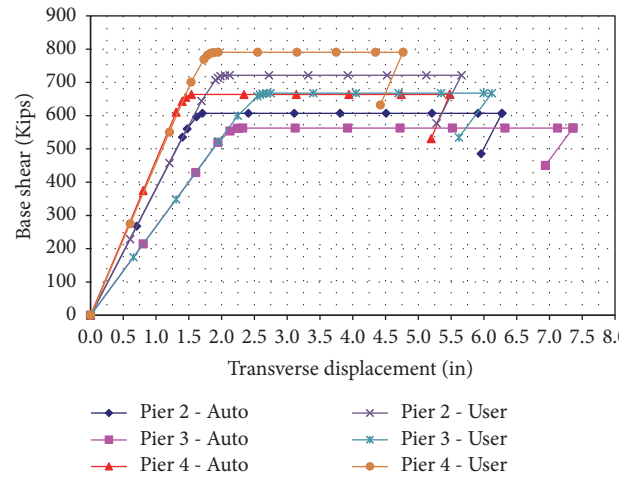

Figure 4: Transverse pushover capacity curve of Bridge #1-W.

7.2. Bridge #2-E. Analysis results showed that the behaviours of Pier #2 and Pier #3 are similar; thus only the deformation capacities for Pier #2 are discussed. Table 10 shows that buckling of longitudinal rebars is the controlling limit state of Pier #2 columns at P_b and P_s axial load levels in the longitudinal and transverse directions. This behaviour is attributed to the poor confinement details, #3 hoops at 12.0 in. spacing. As the axial load level decreases, the value of the plastic curvature capacity increases until the axial load level reaches zero, P_f, whereat compression of the unconfined concrete is the controlling limit state. Table 11 shows the moment-curvature ordinates and the plastic hinge lengths of Pier #2 columns. Similar to the findings for Bridge #1, the

Table 11: User-defined plastic hinge properties of Pier #2 columns, Bridge #2-E.

Direction	Axial load level	Overstrength Axial (kips)	Overstrength Moment (kip·ft)	Plastic hinge length (L_p) (in.)	Yield curvature rad/in$*10^{-6}$	Yield rotation Rad	Plastic curvature rad/in$*10^{-6}$	Plastic rotation Rad
T	P_b	−1543.0	1554.4	17.41	99.6	0.00173	**0.0001173**	0.00204
	P_s	−405.0	1182.2				**0.0004913**	0.00856
	P_f	0.0	870.2				**0.0011457**	0.01995
L	P_b	−1543.0	1554.4	27.37	99.6	0.00273	**0.0001173**	0.00321
	P_s	−302.0	1111.8				**0.0006231**	0.01706
	P_f	0.0	870.2				**0.0011457**	0.03136

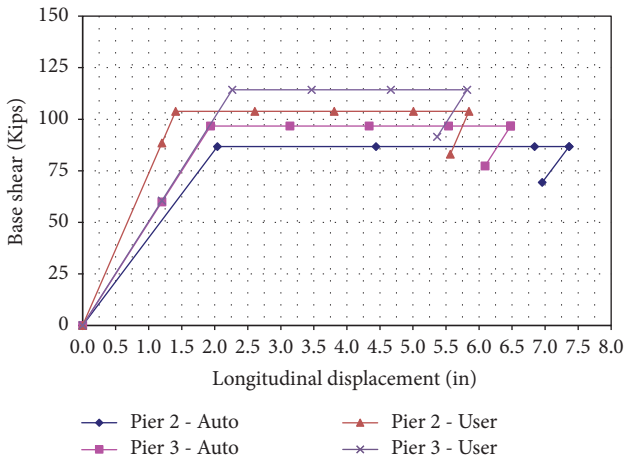

Figure 5: Longitudinal pushover capacity curve of Bridge #2-E.

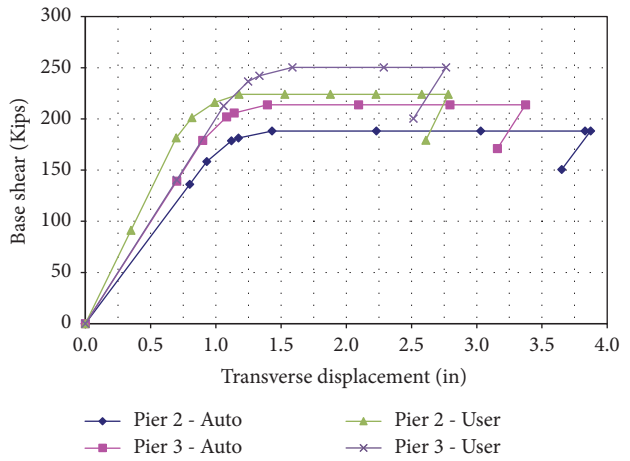

Figure 6: Transverse pushover capacity curve of Bridge #2-E and Bridge #3-E.

change in the type of the controlling limit state supports the effect of the axial load level on the deformation capacity of the plastic hinge. For example, the plastic curvature capacity was equal to 0.0001173 rad/in at axial force of 1543.0 kips and 0.0011457 rad/in. at zero axial force level.

Figures 5 and 6 show the capacity curves of Bridge #2-E in the longitudinal and transverse directions, respectively. Figure 5 shows that the base shear capacity of Pier #2 and Pier #3 in the longitudinal direction using the automated-hinge model is less than base shear capacity using user-defined hinge model by 16.4% and 15.4%, respectively. This difference is basically due to the fact that the idealized flexural capacity in the FHWA-SRM is an overstrength moment which includes an overstrength factor in addition to the factor associated with the expected material properties. The displacement capacity of Pier #2 and Pier #3 in the longitudinal direction using the automated-hinge model is higher than the displacement capacity using user-defined hinge model by 25.9% and 11.3%, respectively. Similarly, Figure 6 shows that base shear capacity of Pier #2 and Pier #3 in the transverse direction using the automated-hinge model is less than base shear capacity using user-defined hinge model by 16.0% and 14.6%, respectively. However, the displacement capacity of Pier #2 and Pier #3 in the transverse direction using the automated-hinge model is higher than the displacement capacity using user-defined hinge model by 39.2% and 22.0%, respectively. A close look at the capacity curves shows higher differences in the displacement capacity in the transverse direction than in the longitudinal direction between the two different hinge models. This difference is due to the fact that the expected seismic and gravity axial load level in the transverse direction is higher than the axial load level in the longitudinal direction which in turn shifts the controlling capacity limit state to buckling of the longitudinal bars. The higher this shift is, the higher the difference between the curvature values obtained from buckling of longitudinal rebars limit state and the failure compression of the unconfined concrete limit state is. The latter is one of the two controlling limit states for the automated-hinge model.

7.3. Bridge #3-E. The pier columns of this bridge are rectangular columns with poor confinement details, #3 hoops at 12.0 in. spacing. Table 12 supports the notion that buckling of longitudinal rebars is the controlling limit state at P_b axial load level as expected from the behaviour of the previous bridges. Compression failure of the unconfined concrete limited the curvature capacity of the columns at P_s axial load level, while low cycle fatigue of longitudinal rebars was the controlling limit state at P_f axial load level. Table 13 shows the user-defined hinge properties of Pier #2 columns, wherein the plastic hinge length has the same value in the longitudinal

Table 12: Plastic curvature capacity of Pier #2 columns, Bridge #3-E.

Axial load level	Axial Force* (kips)	Direction	Compression failure unconfined	Buckling of long. rebars	Fracture of long. rebars	Low-cycle fatigue of long. rebars	Failure in the lap-splice zone
			Rad/in.				
P_b	−1300.1	T & L	0.0003102	**0.0002003**	0.0063260	0.0021910	0.0015229
P_s	−432.0	T	**0.0008436**	0.0011569	0.0044562	0.0021910	0.0023165
P_s	−303.0	L	**0.0010593**	0.0021517	0.0042670	0.0021910	0.0026375
P_f	0.0	T & L	0.0023579	Tension	0.0038788	**0.0021910**	0.0045696

* P_o = −3262.9 kips and P_t = 662.4 kips.

Table 13: User-defined plastic hinge properties of Pier #2 columns, Bridge #3-E.

Direction	Axial load level	Overstrength Axial (kips)	Overstrength Moment (kip·ft)	Plastic hinge length (L_p) (in.)	Yield curvature rad/in∗10^{-6}	Yield rotation Rad	Plastic curvature rad/in∗10^{-6}	Plastic rotation Rad
T & L	P_b	−1300.1	1309.2	19.18	125.0	0.0024	**0.0002003**	0.00384
	P_s	−432.0	1053.0				**0.0008436**	0.01618
	P_f	0.0	734.7				**0.0021910**	0.04202
L	P_s	−303.0	971.3	19.18	125.0	0.0024	**0.0010593**	0.02032

and transverse directions. This is because the shear span is identical in both directions. A comparison between the ultimate curvature capacities of the columns of this bridge and the columns of Bridge #2 shows the effect of the column cross section dimensions on the value of the curvature capacity. For the compression failure of the unconfined concrete limit state at zero axial load level, the plastic curvature capacity was equal to 0.0001173 rad/in for Bridge #2 while the plastic curvature capacity was 0.0023579 rad/in. for Bridge #3. This finding is related to the smaller depth of the column section in Bridge #3 which is equal to 30 in. compared to 36 in. for the columns of Bridge #2. This difference in the section size will support the capability of the smaller column section to undergo higher curvature levels for the same level of concrete strain.

Figures 7 and 8 show the capacity curves of the bridge in the transverse and longitudinal directions, respectively. The capacity curve in the longitudinal direction was obtained for the whole bridge because the soil behind the bridge abutments was part of the seismic load resisting system. According to Figure 7, the displacement capacity of Pier #2, Pier #3, and Pier #4 determined using the automated-hinge model is higher than the displacement capacity using the user-defined model by 0.3%, 0.5%, and 1.6%, respectively. However, the corresponding base shear capacity was lower by 19.2%, 23.4%, and 20.6%, respectively. A similar trend was experienced in the longitudinal direction for the whole bridge with 26.8% and 4.4% difference in the displacement and base shear capacities, respectively. The differences in the capacity curves between the two hinge models are attributed to differences in the moment-curvature values. At an axial load level of −432.0 kips, the ultimate curvature capacity is equal to 1.09×10^{-3} rad/in. and the associated idealized

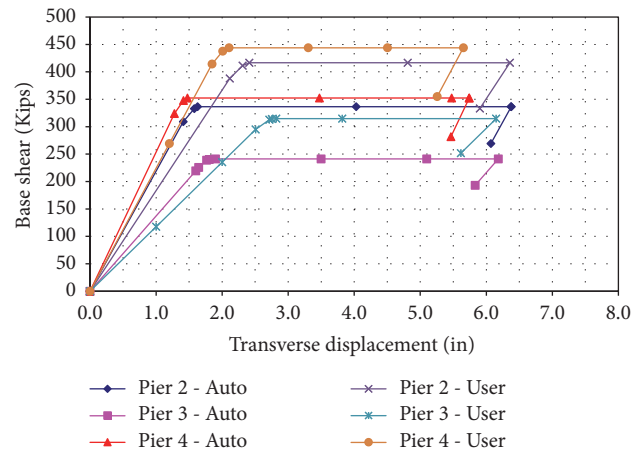

Figure 7: Transverse pushover capacity curve of Bridge #3-E.

moment capacity is equal to 901.3 k·ft using the automated-hinge model in SAP2000. The corresponding values using the user-defined model are equal to 0.84×10^{-3} rad/in. and 1053.0 k·ft, respectively.

7.4. Bridge #4-W. For brevity, the results of Pier #2 widened columns will be discussed. The columns in the widened part of Bridge #4-W were provided by #4 transverse reinforcement at 3.0 in. on centre. However, the longitudinal rebars were spliced within the plastic hinge zone with a length of 40.0 in. Table 14 demonstrates that failure of the confined concrete is the controlling limit state at P_b axial load level, whereas failure in the lap splice zone is the controlling limit state at all other axial load levels.

Table 14: Plastic curvature capacity of new columns, Pier #2 & #3 of Bridge #4-W.

Axial load level	Axial Force* (kips)	Direction	Compression failure confined	Buckling of long. rebars	Fracture of long. rebars	Low-cycle fatigue of long. rebars	Failure in the lap-splice zone
			Rad/in.				
P_b	−1824.8	T & L	**0.0011169**	NC**	0.0056628	0.0019116	0.0011484
P_s	−268.0	T & L	0.0030921	NC	0.0037002	0.0019116	**0.0012960**
P_f	0.0	T & L	0.0046158	NC	0.0034514	0.0019116	**0.0013836**

* P_o = −5264.7 kips and P_t = 1615.2 kips; ** NC = Not controlling.

Table 15: User-defined plastic hinge properties of new columns, Pier #2 Bridge #4-W.

Direction	Axial load level	Overstrength Axial (kips)	Overstrength Moment (kip·ft)	Plastic hinge length (L_p) (in.)	Yield curvature rad/in∗10^{-6}	Yield rotation Rad	Plastic curvature rad/in∗10^{-6}	Plastic rotation Rad
T	P_b	−1824.8	2418.5	25.05	146.4	0.00367	**0.0011169**	0.02798
	P_s	−268.0	1923.1	23.12			**0.0012960**	0.02997
	P_f	0.0	1737.9				**0.0013836**	0.03199
L	P_b	−1824.8	2418.5	37.53	146.4	0.00549	**0.0011169**	0.04191
	P_s	−268.0	1923.1	23.12			**0.0012960**	0.02997
	P_f	0.0	1737.9				**0.0013836**	0.03199

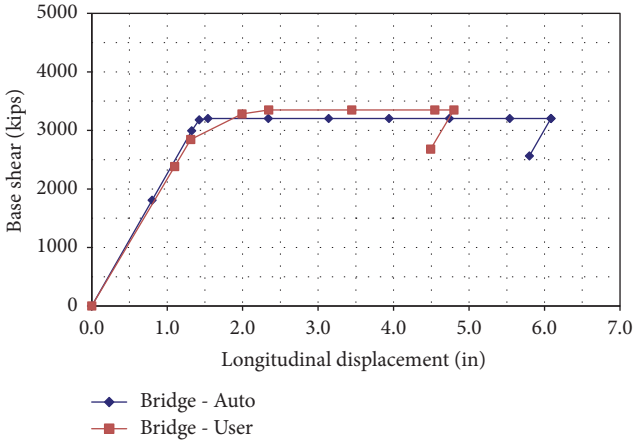

Figure 8: Longitudinal pushover capacity curve of Bridge #3-E.

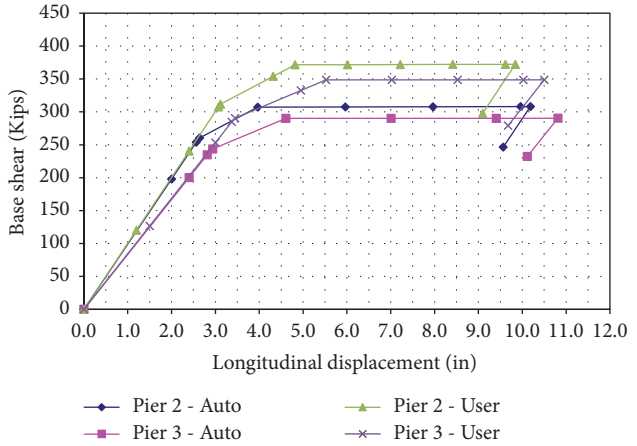

Figure 9: Longitudinal pushover capacity curve of Bridge #4-W.

A comparison between the ultimate curvature capacities of the columns of this bridge and the columns of Bridge #2 shows the effect of the confinement on the value of the curvature capacity. For the compression failure of the unconfined concrete limit state at zero axial load level, the plastic curvature capacity was equal to 0.0001173 rad/in for Bridge #2 while the plastic curvature capacity was 0.0046158 rad/in. for Bridge #4. This finding is related to the huge difference in the details of the transverse reinforcement of the column section in Bridge #2 which has #3 hoops at 12 in. and the transverse reinforcement of the column section in Bridge #4 which has #4 spirals at 3.0 in. This difference in the confinement details will allow the section to undergo higher plastic deformations.

Table 15 includes the nonlinear properties of the user-defined hinge model. It is for the first time that two different plastic hinge lengths are reported for the column in the same direction, as shown in Table 15. This result is pertained to change in the controlling deformation limit state from failure of the confined concrete at P_b axial load level to low cycle fatigue of the longitudinal bars at P_s and P_f axial load levels. Based on the FHWA-SRM, when at the deformation capacity is controlled by low cycle fatigue of longitudinal bars, the effective plastic hinge length is reduced in length and the effective plastic hinge is concentrated at the beginning of the lap. This finding brings attention to the limited capabilities of the lumped plasticity model in dealing with conditions where the plastic hinge length changes with the axial load level.

Figures 9 and 10 show the capacity curves of the bridge in the longitudinal and transverse directions, respectively.

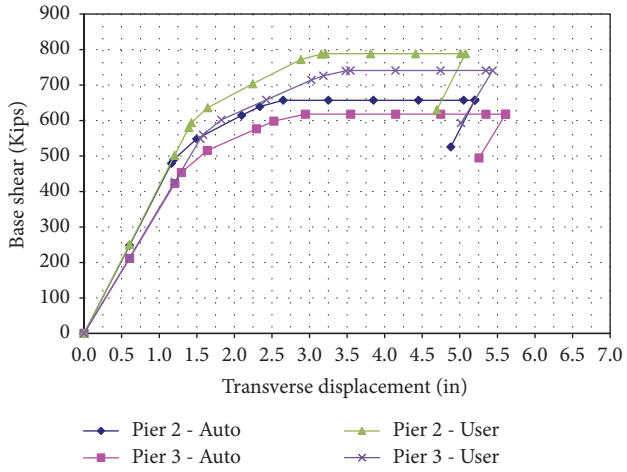

Figure 10: Transverse pushover capacity curve of Bridge #4-W.

According to Figure 9, the displacement capacity of Pier #2 and Pier #3 determined using the automated-hinge model is higher than the displacement capacity using the user-defined model by 3.5% and 3.0%, respectively. However, the corresponding base shear capacity was lower by 17.2% and 16.7%, respectively. A similar trend was experienced in the transverse direction with 2.5% and 3.2% difference in the displacement capacity, and 16.7% and 16.6% difference in the base shear capacity for Pier #2 and Pier #3, respectively.

8. Conclusions

The conclusions of the study may be summarized as follows:

(1) The results of the analyses clearly showed that the capacity curve depends on the plastic hinge properties. The base shear capacity of models with automated hinges is less than the shear capacity of models with user-defined hinge properties. Also, the displacement capacity of models with automated hinges is higher than the shear capacity of models with user-defined hinges.

(2) User-defined hinge model determined using the provisions of the FHWA-SRM is more reliable than the automated-hinge model since it deals with the effect of possible local failure mechanisms within the plastic hinge zone.

(3) Capacity curves of existing and widened highway bridges are impacted approximately in the same manner when using different hinge models.

(4) It is recommended that bridge design manuals clearly ask bridge designers to evaluate the deformation capacities of existing bridges and widened bridges, which have members that do not meet current seismic detailing standards, using the provisions of the FHWA-SRM.

(5) It is recommended that the software industry, like the software SAP2000, includes in its future versions the capability to model plastic hinges that do not meet current seismic detailing standards.

The scope of the present study was limited to flexure dominated conventionally reinforced concrete bridge piers with the plastic hinge length defined in accordance with the FHWA-SRM. Further research needs to be carried out considering shear dominant piers, other types of reinforcement such as shape memory alloys, and other models for plastic hinge lengths.

Conflicts of Interest

The authors declare that there are no conflicts of interest regarding the publication of this paper.

References

[1] M. J. N. Priestley, F. Seible, and G. M. Calvi, *Seismic Design and Retrofit of Bridges*, John Wiley Sons, New York, NY, USA, 1996.

[2] N. K. Shattarat, M. D. Symans, D. I. McLean, and W. F. Cofer, "Evaluation of nonlinear static analysis methods and software tools for seismic analysis of highway bridges," *Engineering Structures*, vol. 30, no. 5, pp. 1335–1345, 2008.

[3] N. Panandikar Hede and K. S. B. Narayan, "Sensitivity of pushover curve to material and geometric modelling—an analytical investigation," *Structures*, vol. 2, pp. 91–97, 2015.

[4] R. Pinho, C. Casarotti, and S. Antoniou, "A comparison of single-run pushover analysis techniques for seismic assessment of bridges," *Earthquake Engineering and Structural Dynamics*, vol. 36, no. 10, pp. 1347–1362, 2007.

[5] R. Pinho, R. Monteiro, C. Casarotti, and R. Delgado, "Assessment of continuous span bridges through nonlinear static procedures," *Earthquake Spectra*, vol. 25, no. 1, pp. 143–159, 2009.

[6] T. Isaković, M. P. Nino Lazaro, and M. Fischinger, "Applicability of pushover methods for the seismic analysis of single-column bent viaducts," *Earthquake Engineering and Structural Dynamics*, vol. 37, no. 8, pp. 1185–1202, 2008.

[7] T. S. Paraskeva, A. J. Kappos, and A. G. Sextos, "Extension of modal pushover analysis to seismic assessment of bridges," *Earthquake Engineering and Structural Dynamics*, vol. 35, no. 10, pp. 1269–1293, 2006.

[8] S. Antoniou and R. Pinho, "Advantages and limitations of adaptive and non-adaptive force-based pushover procedures," *Journal of Earthquake Engineering*, vol. 8, no. 4, pp. 497–522, 2004.

[9] A. S. Elnashai, "Advanced inelastic static (pushover) analysis for earthquake applications," *Structural Engineering and Mechanics*, vol. 12, no. 1, pp. 51–69, 2001.

[10] F. Naeim, *Ten Commandments on Pushover Analysis*, John A. Martin and Associates, Los Angeles, Calif, USA, 1999.

[11] A. K. Chopra and R. K. Goel, *A Modal Pushover Analysis Procedure to estimate Seismic Demands for Buildings: Theory and Preliminary Evaluation*, Pacific Earthquake Engineering Research Center, College of Engineering University of Berkeley, Berkeley, Calif, USA, 2001.

[12] J. Mao, C. Zhai, and L. Xie, "An improved modal pushover analysis procedure for estimating seismic demands of structures," *Earthquake Engineering and Engineering Vibration*, vol. 7, no. 1, pp. 25–31, 2008.

[13] H. Krawinkler and G. D. P. K. Seneviratna, "Pros and cons of a pushover analysis of seismic performance evaluation," *Engineering Structures*, vol. 20, no. 4-6, pp. 452–464, 1998.

[14] FEMA, "NEHRP guidelines for the seismic rehabilitation of buildings," Report FEMA-273 (Guidelines) and Report FEMA-274 (Commentary), Washington, DC, USA, 1997.

[15] ATC, "Seismic evaluation and retrofit of concrete buildings," Tech. Rep. ATC-40, Applied Technology Council, Redwood, Calif, USA, 1997.

[16] FEMA, "Prestandard and commentary for the seismic rehabilitation of buildings," Tech. Rep. FEMA 356, American Society of Civil Engineers for the Federal Emergency Management Agency, Washington, DC, USA, 2000.

[17] CEN, "Eurocode 8: Design of structures for earthquake resistance, Part 1: general rules, seismic actions and rules for buildings," Tech. Rep. EN1998-1, European Committee for Standardization, 2004.

[18] FEMA, "Improvement of nonlinear static seismic analysis procedures," Applied Technology Council (ATC-55 Project) FEMA 440, Federal Emergency Management Agency, Washington, DC, USA, 2005.

[19] ASCE, "Seismic rehabilitation of existing buildings," Tech. Rep. ASCE/SEI 7- 05, American Society of Civil Engineers, 2005.

[20] M. Inel and H. B. Ozmen, "Effects of plastic hinge properties in nonlinear analysis of reinforced concrete buildings," *Engineering Structures*, vol. 28, no. 11, pp. 1494–1502, 2006.

[21] A. H. M. M. Billah and M. Shahria Alam, "Plastic hinge length of shape memory alloy (SMA) reinforced concrete bridge pier," *Engineering Structures*, vol. 117, pp. 321–331, 2016.

[22] K. C. Shrestha, M. S. Saiidi, and C. A. Cruz, "Advanced materials for control of post-earthquake damage in bridges," *Smart Materials and Structures*, vol. 24, no. 2, Article ID 025035, 2015.

[23] A. H. M. Muntasir Billah and M. Shahria Alam, "Performance-based seismic design of shape memory alloy-reinforced concrete bridge piers. I: development of performance-based damage states," *Journal of Structural Engineering*, vol. 142, no. 12, Article ID 4016140, 2016.

[24] CALTRANS, "Caltrans seismic design criteria," Tech. Rep. Version 1.6, California Department of Transportation, 2010.

[25] CSI, "SAP2000: integrated software for structural analysis and design," Tech. Rep. Version 18.2, Computers and Structures, 2016.

[26] FHWA, "Seismic retrofitting manual for highway structures: part 1-bridges," Publication No FHWA-HRT-06-032, Federal Highway Administration, US Department of Transportation, Washington, DC, USA, 2006.

[27] N. Shatarat, "Effect of plastic hinge properties in nonlinear analysis of highway bridges," *Jordan Journal of Civil Engineering*, vol. 6, no. 4, pp. 501–510, 2012.

[28] PTC MathCAD, "Engineering math software," Tech. Rep. Version 15, PTC, Needham, Mass, USA, 2010.

[29] AASHTO, *Guide Specifications for LRFD Seismic Bridge Design*, American Association of State Highway and Transportation Officials (AASHTO), Washington, DC, USA, 2nd edition, 2011, with 2012, 2014, and 2015 Interim Revisions.

[30] J. B. Mander, M. J. N. Priestley, and R. Park, "Theoretical stress-strain model for confined concrete," *Journal of Structural Engineering*, vol. 114, no. 8, pp. 1804–1826, 1988.

[31] Lpile, *A Program for the Analysis of Piles and Drilled Shafts under Later Load*, Version 2014, Ensoft, Austin, Tex, USA, 2014.